Journal of Siberian Federal University. Chemistry 2022 15(4): 457–465
~ ~ ~

DOI: 10.17516/1998-2836-0308

EDN: BRAEOL

УДК 541. 122: 538. 214

Ionic Processes in Pyrochlore-Type $Bi_2Cu_{0.3}Mg_{0.7}Ta_2O_9$

Nadezhda A. Zhuk[*a], Nikolay A. Sekushin[b], Boris A. Makeev[c] and Yana D. Sennikova[c]

[a]Syktyvkar State University
Syktyvkar, Komi Republic, Russian Federation
[b]Institute of Chemistry of the Komi Science Center UB RAS,
Syktyvkar, Republic of Komi, Russian Federation
[c]Institute of Geology of the Komi Science Center UB RAS,
Syktyvkar, Komi Republic, Russian Federation

Received 05.07.2021, received in revised form 23.08.2022, accepted 03.10.2022

Abstract. Cu, Mg-codoped bismuth tantalate pyrochlore was synthesized for the first time by the standard ceramic method. The electrical properties were investigated by impedance spectroscopy in the frequency range 10–10^6 Hz and at a temperature of 25–450 °C. In the investigated frequency range, three polarization processes were recorded for the sample. Simulation of equivalent circuits and calculation of the parameters of electrical models taking into account three types of polarization have been carried out. Low- and mid-frequency polarization has been associated with oxygen and cationic conductivity (bipolar conductivity). At medium and low frequency polarization, the mechanism of particle transfer does not change with a change in temperature. As the temperature rises, the high-frequency process gradually shifts to the high-frequency region outside the observation window.

Keywords: dielectric properties, impedance spectroscopy, pyrochlore.

Citation: Zhuk, N. A., Sekushin, N. A., Makeev, B. A., Sennikova Ya. D. Ionic processes in pyrochlore-type $Bi_2Cu_{0.3}Mg_{0.7}Ta_2O_9$. J. Sib. Fed. Univ. Chem., 2022, 15(4), 457–465. DOI: 10.17516/1998-2836-0308

* Corresponding author E-mail address: nzhuck@mail.ru

Ионные процессы в пирохлоре $Bi_2Cu_{0.3}Mg_{0.7}Ta_2O_9$

Н. А. Жук[а], Н. А. Секушин[б], Б. А. Макеев[в], Я. Д. Сенникова[в]
[а]Сыктывкарский государственный университет Российская Федерация, Сыктывкар
[б]Институт химии Коми НЦ УрО РАН Российская Федерация, Сыктывкар
[в]Институт геологии Коми НЦ УрО РАН Российская Федерация, Сыктывкар

Аннотация. Стандартным керамическим методом впервые синтезирован фазовочистый Cu, Mg-содержащий пирохлор на основе танталата висмута. Электрические свойства исследованы импеданс-спектроскопией в частотном диапазоне 10–10^6 Hz и при температуре 25–450 °C. В исследованном частотном диапазоне для образца зафиксированы три поляризационных процесса. Проведено моделирование эквивалентных схем и расчет параметров электрических моделей с учетом трех типов поляризации. Низко- и среднечастотную поляризацию связали с кислородной и катионной проводимостью (биполярная проводимость). При средне- и низкочастотной поляризации механизм переноса частиц не меняется при изменении температуры. При повышении температуры высокочастотный процесс постепенно смещается в область высоких частот за границу окна наблюдений.

Ключевые слова: диэлектрические свойства, импеданс-спектроскопия, пирохлор.

Цитирование: Жук, Н. А. Ионные процессы в пирохлоре $Bi_2Cu_{0.3}Mg_{0.7}Ta_2O_9$ / Н. А. Жук, Н. А. Секушин, Б. А. Макеев, Я. Д. Сенникова // Журн. Сиб. федер. ун-та. Химия, 2022, 15(4). С. 457–465. DOI: 10.17516/1998-2836-0308

1. Introduction

Oxide pyrochlores with the general formula $A_2B_2O_6O'$ are currently being thoroughly studied due to their promising practically useful properties. Pyrochloric materials exhibit a wide range of electrical properties, from dielectrics to superconductors. Materials based on them are used in resistors, thermistors, capacitors, in the manufacture of heterogeneous LTCC modules, electronic devices for the microwave range [1,2]. In the crystal structure of pyrochlore (space group Fd-3m), two interpenetrating and independent cationic sublattices A_2O 'and B_2O_6 are distinguished, in which relatively small B (Ta, Nb) cations have octahedral coordination, and large A (Bi, Pb) ions are coordinated in eight vertices [3]. The tolerance of the crystal structure of pyrochlore to vacancies in the anionic and cationic sublattices provides a wide compositional variety of compositions within a given structural type [4,5]. Recently, bismuth-containing pyrochlores have attracted great research interest due to their relatively low sintering temperature and excellent dielectric properties – high dielectric constant and low dielectric losses. For pyrochlores in the Bi_2O_3-Ta_2O_5-CuO (BCT) system, the concentration range of the compositions

$Bi_{2.48+y}Cu_{1.92-x}Ta_{3.6+x-y}O_{14.6+3x/2-y}$: 0≤x≤0.8 and 0≤y≤0.6 [6]. With an increased content of bismuth, monoclinic zirconolite $Bi_{1.92}Cu_{0.08}(Cu_{0.3}Ta_{0.7})_2O_{7.06}$, a structural analog of the β-phase $Bi_2(Zn_{1/3}Ta_{2/3})_2O_7$ [7], is formed. It was found that all cubic BCT pyrochlores exhibit similar electrical behavior and are characterized by moderate values of dielectric constant ε~60–80 and low dielectric losses tanδ~0.01–0.2 (RT, 1 MHz), comparable for pyrochlores of bismuth-magnesium tantalate ~ 80) [6,8]. In [9], a series of nonstoichiometric samples $Bi_{3-x}Cu_{1.8}Ta_{3+x}O_{13.8+x}$(x = 0–0.6) with a pyrochlore structure (BCT) is characterized. These materials are thermally stable up to 900 °C and exhibit semiconducting properties at high temperatures. The tangent of losses increases with increasing temperature. The substitution of zinc atoms for copper in the $Bi_{3.08}Cu_{1.84-x}Zn_xTa_{3.08}O_{14.16}$ system (0≤x≤1.84) led to the formation of thermally stable pyrochlores, which demonstrated a transition from semiconducting to dielectric properties [10]. The activation energy of the materials varied from 0.40 to 1.40 eV, and the dielectric permeability varied in an integral of 50–70, and the loss tangent was limited to the range 10^{-3}–10^{-2} (1 MHz and 25 °C). Magnesium-containing pyrochlores $Bi_{3+5/2x}Mg_{2-x}Ta_{3-3/2x}O_{14-x}$ (0.12≤x≤0.22) showed relatively high values of ε ~ 70–85; the dielectric loss tangent was ~ 10^{-3} (1 MHz and 30 °C) and varied in the range of values from –158 to –328 ppm /°C negative temperature coefficient of capacitance [8,11].

In this article, we declare the synthesis of pure phase pyrochlore with the composition $Bi_2Cu_{0.3}Mg_{0.7}Ta_2O_9$, which exhibits three polarization processes. The nature of ionic processes is investigated by the method of impedance spectroscopy; for each temperature region, an equivalent circuit is modeled, which describes the electrical characteristics of the sample.

2. Experimental

Ceramics with the composition $Bi_2Cu_{0.3}Mg_{0.7}Ta_2O_9$ were synthesized from a stoichiometric mixture of Bi(III), Ta(V), Mg(II), and Cu(II) oxides by the solid-phase method. The stoichiometric mixture was thoroughly ground in an agate mortar in the presence of ethyl alcohol until a homogeneous mass was obtained (at least 1 hour). Thin disks 10–15 mm in diameter were prepared from the obtained homogeneous mixture using a hand-held plexiglass press. The samples were calcined in four stages at 650, 850, 950 and 1050 ˚C for 40 hours. After each calcination, the samples were ground again and discs were prepared. X-ray diffraction patterns of the samples were obtained in the 2-theta range of 10–70° at a scanning speed of 2.0 deg/min using a Shimadzu 6000 X-ray diffractometer (CuKα radiation). The microstructure and local chemical composition of the samples were studied by scanning electron microscopy and energy dispersion X-ray spectroscopy (electron scanning microscope Tescan VEGA 3LMN, energy dispersion spectrometer INCA Energy 450). A conductive silver layer was applied to the lateral surfaces of the samples in the form of disks for the purpose of studying the electrical properties (thickness 2 mm, diameter 13.4 mm). The impedance hodographs were measured using a Z-1000P impedance meter and an E 7–28 immitance analyzer. The temperature control of the samples in the measuring cell was carried out using a chromel-alumel thermocouple (temperature measurement accuracy ± 1 °C).

3. Results and discussion

According to the data of X-ray phase analysis, the sample with the composition $Bi_2Cu_{0.3}Mg_{0.7}Ta_2O_9$ is phase-pure. The X-ray diffraction pattern shows only reflections of the cubic pyrochlore phase (space group *Fd-3m*). The unit cell parameter was 10.5497 Å, which is somewhat larger than the lattice constant for pyrochlore with the composition $Bi_2MgTa_2O_9$ [12] and may be associated with the replacement of smaller Mg (II) ions by Cu (I, II) ions ($R(Ta(V))_{c.n.-6}$=0.64 Å, $R(Cu(II))_{c.n.-6}$=0.73 Å, $R(Cu(I))_{c.n.-6}$=0.77 Å, $R(Mg(II))_{c.n.-6}$=0.72 и $0.89_{c.n.-8}$ Å, $R(Bi(III))_{c.n.-8}$=1.17 Å) [13].

Microstructure analysis by scanning electron microscopy showed that the sample is porous, consisting of intergrown irregular grains with an average transverse size of 2–4 μm (Fig. 2).

As a result of the EDS analysis, it was found that copper atoms are included in the chemical composition of the sample (Fig.2).

In Fig. 3 shows the designations of the frequencies of the maxima (Ω_{max}), which are present in the graphs of the imaginary part of the impedance (–Z″). Frequencies are expressed in either Hz (no Hz symbol) or kHz (there is a k after the number). Ω_{max} carries information about the speed of the polarization process. The characteristics of the medium are also the dependences of the phase of the impedance (φ) on the frequency (Fig. 4).

As can be seen from Fig. 3 and 4, the samples are characterized by three polarization processes: high frequency (high frequency – hf), medium frequency (middle frequency – mf) and low frequency (low frequency – lf). Elements of hodographs have the shape of a semicircle, arcs with constant curvature, and also at T>250°, in the low-frequency region, fragments with variable curvature were

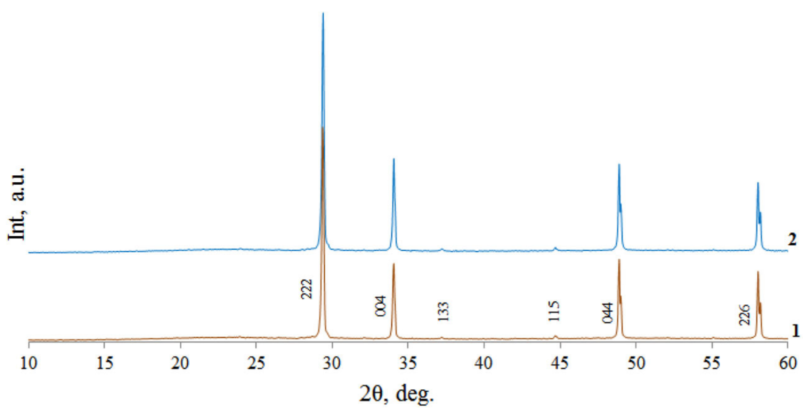

Fig. 1. X-ray diffraction patterns of the $Bi_2MgTa_2O_9$ (1) and $Bi_2Cu_{0.3}Mg_{0.7}Ta_2O_9$ (2)

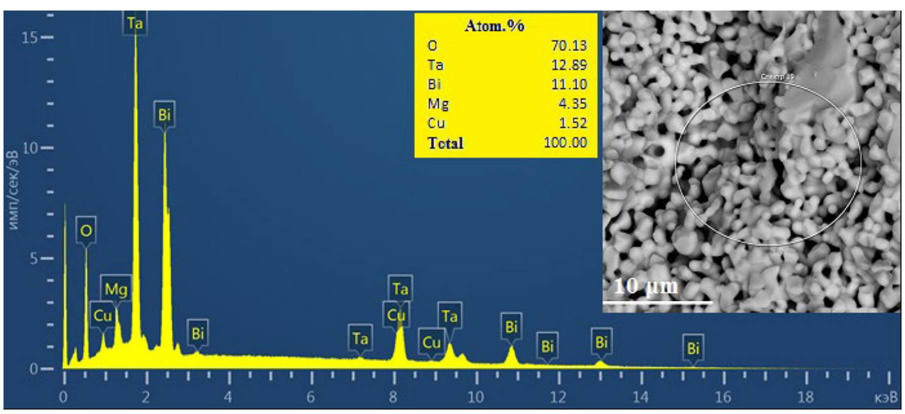

Fig. 2. Microphotograph and EDS spectrum of the $Bi_2Cu_{0.3}Mg_{0.7}Ta_2O_9$

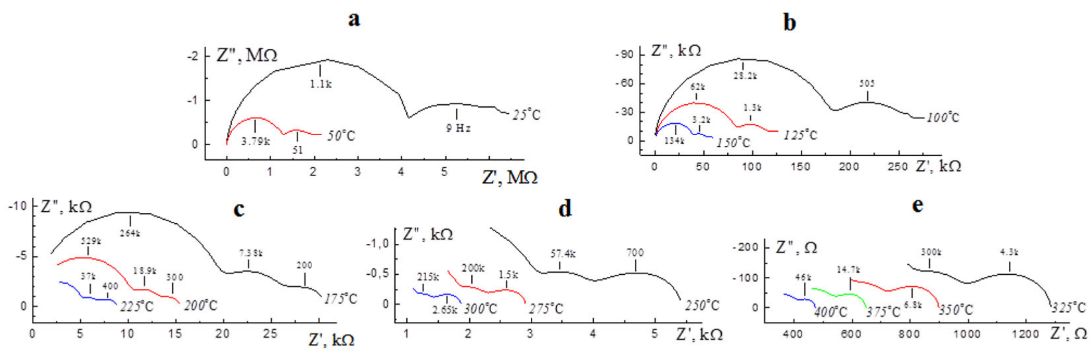

Fig. 3 Hodographs of sample at 25; 50; 100; 125; 150; 175; 200; 225; 250; 275; 300; 325; 350; 375 and 400 °C

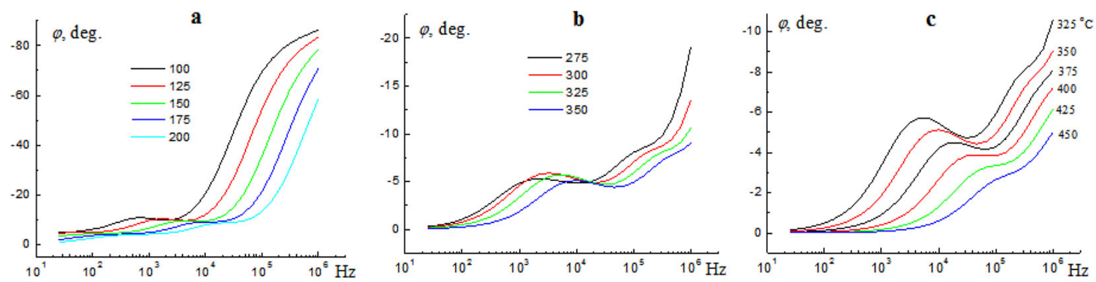

Fig. 4. Frequency dependences of the phase of the impedance of the $Bi_2Cu_{0.3}Mg_{0.7}Ta_2O_9$ at 100; 125; 150; 175; 200; 275; 300; 325; 350; 375; 400; 425 and 450 °C

found, the shape of which resembles a drop cut in half (Fig.3d and 3e). When modeling Nyquist curves with such a feature, models with a drop-shaped hodograph can be used – these are the Gerischer impedance (GE) and the Generalized Finite Warburg element GFW with a transmissive boundary (Transmissive Boundary, designation Ws). In the $Bi_2Cu_{0.3}Mg_{0.7}Ta_2O_9$ sample under study, the selection of adequate ES elements can be carried out by enumerating several ES variants, including either GE or Ws. Evaluation of the ES accuracy is carried out both visually according to the graphs and according to the integral accuracy criteria [14]. We used criterion 2. If χ^2 <0.0001, then the frequency characteristics calculated from the ES practically coincide with similar experimental dependences.

We have found that using Ws instead of GE improves model accuracy by 30 %. The results of modeling the impedance of samples in the temperature range of 25–450° are shown in Fig. 5.

All elements of the ES in Fig. 5 have a certain physical meaning. Resistor Ro is responsible for end-to-end conductivity in ES*a* and ES*b*. Through resistance in ES*c* and ES*d* is equal to the sum of

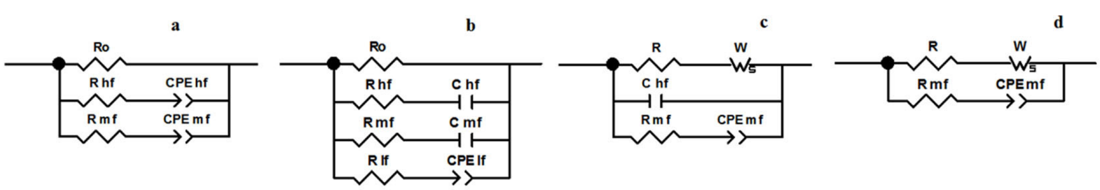

Fig. 5. Equivalent circuits of the $Bi_2Cu_{0.3}Mg_{0.7}Ta_2O_9$ at 25–125 °C (a); 175–225 °C (b); 225–400 °C (c) and 400–450 °C (d)

R+(W-R). The RF polarization process is modeled by the R_{hf} ×CPE_{hf} (ES*a*), R_{hf} ×C_{hf} (ES*b*) and C_{hf} (ES*c*) chains. The CPE constant phase element has two parameters: T_{CPE} and P [15]. At P = 1, the CPE element becomes a capacitor C. As the temperature rises, the RF process gradually shifts to the high-frequency region beyond the observation window boundary. As a result, the number of points on which the ES is built decreases. This leads to an increase in the error in determining the value of some parameters of the electrical model. Therefore, the HF part of the ES has to be gradually simplified. The MF polarization process is confidently observed at all temperatures. It is modeled by the R_{mf} ×CPE_{mf} chain (ES*a*, ES*c* and ES*d*), as well as by the R_{mf} ×C_{mf} (ES*b*) chain. The LF polarization process is not observed at t=25–125 °C. In the temperature range 175–225 °C, the LF polarization is simulated by the R_{lf} ×CPE_{lf} (ES*b*) circuit, and upon subsequent heating, by R×Ws (ES*s* and ES*d*). The ES parameters are given in Tables 1–4.

Such a study can include the construction of various frequency characteristics and the determination of the integral parameters of the environment. In Fig. 6 shows the temperature dependences of the

Table 1. Parameters of Es*a*

t, °C	R_0, Ω	R_{hf}, Ω	$T_{CPE\ hf}$	$P_{CPE\ hf}$	R_{mf}, Ω	$T_{CPE\ mf}$	$P_{CPE\ mf}$	χ″×10⁴
1	2	3	4	5	6	7	8	9
25	$7.17·10^6$	-630	$4.07·10^{-11}$	0.969	$9.09·10^6$	$6.19·10^{-9}$	0.65	26
52	$2.05·10^6$	–671	$4.56·10^{-11}$	0.96	$3.5·10^6$	$1.53·10^{-9}$	0.859	21
100	$2.69·10^5$	–193	$4.81·10^{-11}$	0.959	$5.86·10^5$	$1.01·10^{-9}$	0.899	0.5
125	$1.21·10^5$	–99	$4.92·10^{-11}$	0.959	$2.72·10^5$	$1.76·10^{-9}$	0.847	2.6

Table 2. Parameters of ES*b*

t. °C	R_o. Ω	R_{hf}. Ω	C_{hf}. pF	R_{mf}. Ω	C_{mf}. pF	R_{lf}. Ω	$T_{CPE\ lf}$	$P_{CPE\ lf}$	χ″×10⁴
1	2	3	4	5	6	7	8	9	10
175	34250	261	27.3	1.67e5	119	47053	$1.10·10^{-6}$	0.293	2.6
200	16104	266	27.8	86889	91	37396	$4.03·10^{-7}$	0.426	2.5
225	8914	323	28.3	25815	174	24636	$1.10·10^{-7}$	0.690	1.4

Table 3. Parameters of ES*c*

t. °C	*R*. Ω	W_s-R. Ω	W_s-T. s	W_s-P	C_{hf}. pF	R_{mf}. Ω	$T_{CPE\ mf}$	$P_{CPE\ mf}$	χ″×10⁴
1	2	3	4	5	6	7	8	9	10
225	6547	2285	0.00126	0.400	27.6	22211	$1.26·10^{-9}$	0.850	1.2
250	3774	1672	$7.74·10^{-4}$	0.4	27.5	15367	$5.33·10^{-10}$	0.908	0.7
275	2293	726	$3.23·10^{-4}$	0.408	27.1	10340	$5.23·10^{-10}$	0.894	0.5
300	1349	520	$2.06·10^{-4}$	0.41	26.8	7040	$2.96·10^{-10}$	0.931	0.3
325	946	341	$1.23·10^{-4}$	0.421	24.1	4684	$3.84·10^{-10}$	0.912	0.5
350	691	208	$6.67·10^{-5}$	0.428	20.5	3337	$4.60·10^{-10}$	0.895	0.5
375	523	125	$3.56·10^{-5}$	0.435	13.3	2097	$7.9·10^{-10}$	0.854	0.5
400	402	71.4	$1.77·10^{-5}$	0.444	13.9	1890	$4.95·10^{-10}$	0.879	0.5

Table 4. Parameters of ES*d*

T. °C	*R*. Ω	W_s-R. Ω	W_s-T. s	W_s-P	R_{mf}. Ω	$T_{CPE\ mf}$	$P_{CPE\ mf}$	$\chi''\times10^4$
1	2	3	4	5	6	7	8	9
400	409	64.4	$1.82\cdot10^{-5}$	0.455	854	$3.77\cdot10^{-9}$	0.756	0.6
425	313	46.2	$8.83\cdot10^{-6}$	0.429	1125	$3.01\cdot10^{-10}$	0.905	1.3
450	252	33.7	$4.42\cdot10^{-6}$	0.405	1564	$2.69\cdot10^{-11}$	1	6

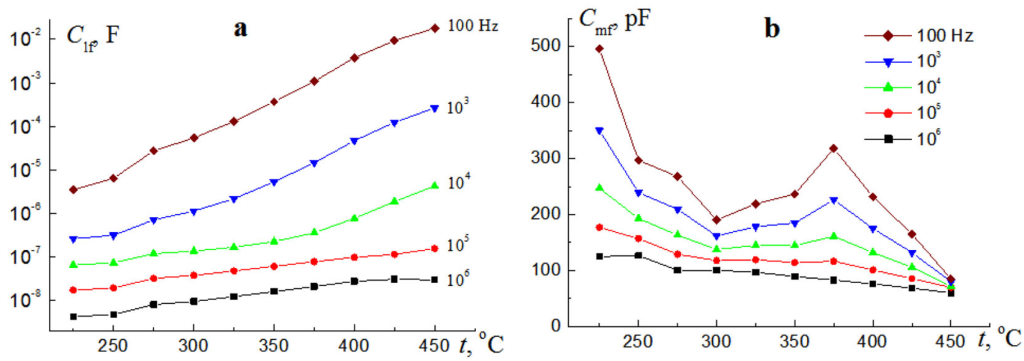

Fig. 6. Temperature dependences of the capacitance of the LF process (a) and the MF process (b) at 0.1. 1. 10. 100. and 1000 kHz

capacities of the LF and MF processes. Capacities are specified for a series equivalent circuit. In this case, the Ws element is replaced with a sequential two-terminal device "C_{lf}×R_{lf}" (lf – low frequency) and CPE – a two-terminal device "C_{mf}×R_{mf}" (mf – middle frequency).

Fig. 6 it follows that both processes under study are due to the transfer of ions, since a fairly strong dispersion is observed. Complex oxide materials especially those with a pyrochlore structure contain both cationic vacancies and vacancies in the oxygen sublattice. Consequently, bipolar ionic conductivity is possible in the $Bi_2Cu_{0.3}Mg_{0.7}Ta_2O_9$ solid solution. It follows from the chemical composition of the compound that the concentration of mobile copper cations is significantly lower than the concentration of mobile oxygen anions. On the other hand it follows from the literature that the conductivity for copper can have a significant value even at room temperature and the conductivity for oxygen is recorded at higher temperatures (> 250°) [16–18]. Thus, the LF polarization process is most likely associated with oxygen conductivity, while the MF process is due to the transfer of copper cations.

In Fig. 7a shows the temperature dependences of the through-going specific conductivity of the substance σ and the time constant τmf on the Arrhenius scale. The points are obtained from the parameters of the equivalent circuits (Fig. 5. Tables 1–4) and formulas (6, 7). The lines are drawn using the least squares method. Activation energies are determined from the tangent of the slope of the lines: E_σ = (0.450±0.005) eV; E_τ = (0.54±0.01) eV.

The Fig. 7a it follows that for MF and LF polarization. The mechanism of particle transfer does not change with a change in temperature. The same conclusion can be drawn from Fig. 7b which shows the temperature dependence of the W_s-T parameter. The numerical values of which are taken from Tables 3 and 4 (column 4). At low-frequency polarization the motion of particles proceeds according

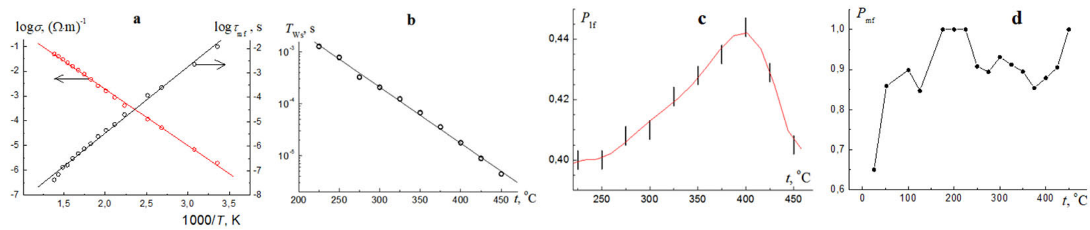

Fig. 7. Temperature dependences of the through conductivity (σ) and the time constant of the MF polarization process (t_{mf}) plotted on the Arrhenius scale (a); Dependences of the parameters W_s-T (b) and W_s-P (c), P_{mf} (d) on temperature (d)

to the diffusion mechanism. Since the W_s-P parameter is close to 0.5 (Fig. 7c). The diffusion rate is directly proportional to the temperature. MF polarization proceeds according to a different mechanism since the P_{CPE} parameter has a value close to 1 (Fig. 7d). The graph is constructed from the data of Tables 1–4 of the midrange polarization.

In this case, the driving force is the electric field under the influence of which the particles make oscillatory movements between the electrodes.

4 Conclusions

The bipolar ionic conductivity $Bi_2Cu_{0.3}Mg_{0.7}Ta_2O_9$ was found in the solid solution. At room temperature ion-migration polarization with the participation of copper cations is observed. At temperatures above 175 °C a second ion-migration mechanism of polarization occurs with the participation of oxygen anions and at 225 °C and above a through oxygen current appears. With a subsequent increase in temperature the cationic conductivity is suppressed. This is due to the fact that the coexistence of two oppositely charged current carriers is unstable.

References

1. Yu, S., Li, L., Zheng, H. BMN-based transparent capacitors with high dielectric tunability. *Alloys Comp.* 2017, 699, 68–72.

2. Guo, Q., Li, L., Yu, S., Sun, Z., Zheng, H., Li, J., Luo, W. Temperature-stable dielectrics based on Cu–doped $Bi_2Mg_{2/3}Nb_{4/3}O_7$ pyrochlore ceramics for LTCC. *Ceram. Intern.* 2018, 44, 333–338.

3. Subramanian, M.A., Aravamudan, G., Subba Rao, G.V. Oxide pyrochlores – a review. *Prog. Solid State Chem*. 1983, 15, 55–143.

4. Zou, Z., Ye, J., Arakawa, H. Preparation, structural and optical properties of a new class of compounds Bi_2MNbO_7 (M=Al. Ga. In). *Mater. Sci. Engineer.* 2001, 79, 83–85.

5. Matteucci, F., Cruciani, G., Dondi, M., Baldi, G., Barzanti, A. Crystal structural and optical properties of Cr-doped $Y_2Ti_2O_7$ and $Y_2Sn_2O_7$ pyrochlores. *Acta Mater.* 2007, 55, 2229–2238.

6. Chon, M.P., Tan, K.B., Khaw, C.C., Zainal, Z., Taufiq-Yap, Y.H., Chen, S.K., Tan, P.Y. Subsolidus phase equilibria and electrical properties of pyrochlores in the Bi_2O_3–CuO–Ta_2O_5 ternary system. *J. Alloys Comp.* 2016, 675, 116–127.

7. Tan, K.B., Chon, M.P., Khaw, C.C., Zainal, Z., Taufiq Yap, Y.H., Tan, P.Y. Novel monoclinic zirconolite in Bi_2O_3–CuO–Ta_2O_5 ternary system: Phase equilibria. structural and electrical properties. *J. Alloys Compd*. 2014, 592, 140–149.

8. Tan, P.Y., Tan, K.B., Khaw, C., Zainal, Z., Chen, S.K., Chon, M.P. Structural and electrical properties of bismuth magnesium tantalate pyrochlores. *Ceram. Intern.* 2012, 38, 5401–5409.

9. Chon, M.P., Tan, K.B., Khaw, C.C., Zainal, Z., Taufiq-Yap, Y.H., Tan, P.Y. Synthesis, structural and electrical properties of novel pyrochlores in the Bi_2O_3–CuO–Ta_2O_5 ternary system. *Ceram. Intern.* 2012, 38, 4253–4261.

10. Chon, M.P., Tan, K.B., Zainal, Z., Taufiq-Yap, Y.H., Tan, P.Y., Khaw, C.C., Chen, S.K. Synthesis and Electrical Properties of Zn-substituted Bismuth Copper Tantalate Pyrochlores. Intern. *J. Appl. Ceram. Techn.* 2016, 13, 718–725.

11. Tan, P.Y., Tan, K.B., Khaw, C.C., Zainal, Z., Chen, S.K., Chon, M.P. Phase equilibria and dielectric properties of $Bi_{3+(5/2)x}Mg_{2-x}Nb_{3-(3/2)x}O_{14-x}$ cubic pyrochlores. *Ceram. Intern.* 2014, 40, 4237–4246.

12. Zhuk, N.A., Krzhizhanovskaya, M.G., Sekushin, N.A., Kharton, V.V., Makeev, B.A., Belyy, V.A., Korolev, R.I. Dielectric performance of pyrochlore-type $Bi_2MgNb_{2-x}Ta_xO_9$ ceramics: The effects of tantalum doping. *Ceram. Intern.* 2021, 47, 194247–19433.

13. Shannon, R.D. Revised effective ionic radii and systematic studies of interatomic distances in halides and chalcogenides. *Acta Crystallogr.* A. 1976, 32, 751–767.

14. Lasia, A. Electrochemical impedance spectroscopy and its applications. New York: Springer Science+Business Media, 2014. 369 p.

15. Barsoukov, E., Macdonald, J.R. Impedance spectroscopy: theory, experiment and application. Wiley – Interscience, 2005. 606 p.

16. Zhuk, N.A., Sekushin, N.A., Makeev, B.A. Impedance spectroscopy of $Bi_{1.6}Mg_{0.24}Cu_{0.56}Ta_{1.6}O_{7.2.}$ *Lett. Mater.* 2021, 11, 11–16.

17. Zhuk, N.A., Sekushin, N.A., Krzhizhanovskaya, M.G., Belyy, V.A., Korolev, R.I. Electrical properties of Ni-doped $CaCu_3Ti_4O_{12}$ ceramics. *Sol. St. Ion.* 2021, 364, 115633.

18. Sekushin, N.A., Zhuk, N.A., Koksharova, L.A., Belyy, V.A., Makeev, B.A., Beznosikov, D.S., Yermolina, M.V. Impedance spectroscopy study of the electrical properties of composites of $CaCu_3Ti_4O_{12}$-CuO. *Lett. Mater.* 2019, 9, 5–10.